crystals

MDPI

Article

Experimental Investigation and Prediction of Mechanical Properties in a Fused Deposition Modeling Process

Amanuel Diriba Tura [1], Hirpa G. Lemu [2,*] and Hana Beyene Mamo [1]

[1] Faculty of Mechanical Engineering, Jimma University, MVJ4+R95 Jimma, Ethiopia; diriba.amanuel@ju.edu.et (A.D.T.); hanicho2102@gmail.com (H.B.M.)
[2] Faculty of Science and Technology, University of Stavanger, N-4036 Stavanger, Norway
* Correspondence: hirpa.g.lemu@uis.no

Abstract: Additive manufacturing, also known as three-dimensional printing, is a computer-controlled advanced manufacturing process that produces three-dimensional items by depositing materials directly from a computer-aided design model, usually in layers. Due to its capacity to manufacture complicated objects utilizing a wide range of materials with outstanding mechanical qualities, fused deposition modeling is one of the most commonly used additive manufacturing technologies. For printing high-quality components with appropriate mechanical qualities, such as tensile strength and flexural strength, the selection of adequate processing parameters is critical. Experimentally, the influence of process parameters such as the raster angle, printing orientation, air gap, raster width, and layer height on the tensile strength of fused deposition modeling printed items was examined in this work. Through analysis of variance, the impact of each parameter was measured and rated. The system's response was predicted using an adaptive neuro-fuzzy technique and an artificial neural network. In Minitab software, the Box-Behnken response surface experimental design was used to generate 46 experimental trials, which were then printed using acrylonitrile butadiene styrene polymer materials on a three-dimensional forge dreamer II fused deposition modelling printing machine. The results revealed that the raster angle, air gap, and raster width had significant impacts on the tensile strength. The adaptive neuro-fuzzy approach and artificial neural network predicted tensile strength accurately with an average percentage error of 0.0163 percent and 1.6437 percent, respectively. According to the findings, the model and experimental data are in good agreement.

Keywords: fused deposition modeling; mechanical properties; tensile strength; adaptive neuron-fuzzy methods; artificial neural network

Citation: Tura, A.D.; Lemu, H.G.; Mamo, H.B. Experimental Investigation and Prediction of Mechanical Properties in Fused Deposition Modeling Process. *Crystals* **2022**, *12*, 844. https://doi.org/10.3390/cryst12060844

Academic Editors: Hao Yi, Huajun Cao, Menglin Liu and Le Jia

Received: 15 May 2022
Accepted: 13 June 2022
Published: 15 June 2022

1. Introduction

Additive manufacturing is a novel technology that uses a layer-based production method to create a product straight from a computer-aided design model (CAD) model. Fused deposition modeling (FDM) is one of several three-dimensional (3D) printing techniques that employ flexible thermoplastic filament injected through a heated nozzle to build components. The thermoplastics and reinforced thermoplastic materials that can be printed with FDM include acrylonitrile butadiene styrene (ABS), polylactic acid (PLA), polycarbonate, unfilled polyetherimide (PEI), Polyether ether ketone (PEEK), Polyethylene terephthalate glycol (PETG), and fiber-reinforced thermoplastics. FDM-produced components are increasingly displacing conventional components in a variety of industries, including the automotive, aviation, and medical sectors [1–5]. The process variables and their settings have a substantial impact on the mechanical qualities of FDM-printed components. As a result, enhancing the mechanical qualities of printed components requires analyzing the effects of input factors and anticipating results by using adequate settings [6–9].

Several studies and predicted models of the impact of printing settings on the mechanical qualities of FDM components have been conducted by various scholars using various approaches such as the adaptive neuro-fuzzy technique (ANFIS), artificial neural network (ANN), response surface method (RSM), analysis of variance (ANOVA), group method for data handling (GMDH), and differential evolution (DE). According to Zhou, et al. [10], the infill density and printing pattern, for example, had a substantial impact on the tensile strength of polylactic acid FDM-printed components. Gebisa and Lemu [11] investigated the impact of process factors such as air gap, raster size, raster angle, contour quantity, and contour width on the tensile characteristics of components manufactured using the FDM technique and ULTEM 9085 polymeric material. According to their research, the raster angle has a significant effect on tensile properties. Byberg, et al. [12] looked at how layer alignment and build direction influenced the mechanical qualities of ULTEM 9085 thermoplastic. According to their results, the layer orientations and construction directions had a huge impact on the mechanical characteristics of the polymer.

The impact of principal directions, inclination angle, and air separation on the flexural characteristics of ULTEM 9085 fabricated by using the FDM technique with both solid and sparse building methods was examined by Motaparti, et al. [13]. Their study revealed that vertical (edge) designs had a greater elastic yield point than horizontal ones. According to Gebisa and Lemu [14], raster angle and width have a significant impact on the ULTEM 9085 polymer's flexible pavements. The impact of process parameters (layer height and printing speed) on the mechanical characteristics of 3D-printed ABS composite was investigated by Christiyan, et al.[15]. They revealed that the material's optimal tensile and flexural strength were achieved while using a low production speed and a minimal layer height. Hsueh, et al. [16] studied how FDM process factors impacted the mechanical characteristics of PLA and PETG materials (printing temperatures and rates). The results reveal that when the printing temperature increases, the PLA and PETG materials' mechanical characteristics (tension, compression, and bending) are enhanced. Furthermore, when manufacturing speed rises, the PLA material's mechanical behavior improves while the mechanical features of the PETG material deteriorate. According to Enemuoh, et al. [17], infill density has a significant impact on the tensile properties of the FDM component, followed by layer, speed, and infill patterns. Hsueh, et al. [18] investigated the impact of printing temperature and infill rate on the mechanical characteristics of FDM-printed PLA components using tensile and Shore D hardness tests. Raising the infill proportion or printing temperature, according to their results, could dramatically improve the material's longitudinal elastic modulus, ultimate strength, elasticity, and Shore hardness.

Patil, et al. [19] evaluated the tensile and flexural strength of FDM-printed PLA components using experimental testing and finite element analysis. Using 33 trials and result data, Manoharan, et al. employed ANN to develop mathematical models for predicting the tensile properties of FDM-made PLA components. The observed tensile strength results were compared to the anticipated values using the RSM, ANN, and ANOVA findings. Pazhamannil and Govindan [20] used an artificial neural network to estimate the tensile properties of FDM-printed items at various nozzle temperatures, layer thicknesses, and infill rates. Rayegani and Onwubolu [21] used DE and the GMDH to predict and optimize the link between FDM component strength properties and operating parameters (part alignment, inclination angle, raster size, and air gap). Srinivasan, et al. [22] employed response surface methodology to predict and optimize the impact of process factors on tensile properties of FDM-produced ABS components.

According to the literature, pre-processing settings have a considerable effect on the mechanical features of FDM-produced parts. It was also crucial to examine the combined influence of FDM settings on the mechanical features of produced components. As a result, five crucial pre-processing parameters (raster angle, printing orientation, air gap, raster width, layer height) were chosen as inputs for the current study: The tensile strength

characteristics (UTS) were selected as the output response. Furthermore, the application of ANFIS and ANN was used to predict the response output, validated with experimental results.

2. Materials and Methods

2.1. 3D Printer and Materials

A Flash Forge Guider II 3D printer was used to create the specimens in this study. The build envelope of the printer measures 280 × 250 × 300 mm^3 and can generate components with 0.2 mm accuracy. The 3D printer's characteristics are shown in Table 1. The study employed ABS printing materials since it is a strong thermoplastic and a typical FDM material. ABS is best suited for parts that require strength and flexibility, such as car components or household appliances. ABS is synthesized using three monomers: acrylonitrile, butadiene, and styrene, in an emulsion or continuous mass process. Acrylonitrile is a chemically resistant and thermally stable synthetic monomer made from propylene and ammonia that is used to make ABS. Butadiene is a by-product of ethylene synthesis from steam crackers that gives ABS polymer hardness and impact strength. ABS plastic gets its stiffness and processability from styrene, which is made by dehydrogenating ethyl benzene. Acrylonitrile butadiene styrene has the chemical formula $C_8H_8{\cdot}C_4H_6{\cdot}C_3H_3N$ [23–26]. ABS has a low melting point, which enables it to be easily used in 3D printing. It is very resistant to physical impacts and chemical corrosion, which allows the finished plastic to withstand heavy use and adverse environmental conditions [27,28]. The mechanical properties of the printing materials are shown in Table 2.

Table 1. The specification of the Flash Forge Guider II 3D printer.

Name	Guider II
Number of extruder	1
Print technology	Fused deposition modeling (FDM)
Build volume	280 × 250 × 300 mm
Layer resolution	0.05–0.4 mm
Build accuracy	±0.2 mm
Positioning accuracy	Z axis 0.0025 mm; XY axis 0.011 mm
Filament diameter	1.75 mm (±0.07)
Nozzle diameter	0.4 mm
Nozzle temperature	210–250 °C
Platform temperature	0–120 °C
Print speed	10–200 mm/s

Table 2. The specification of the ABS printing materials.

Properties	Specification
Material	ABS
Color	White
Wire diameter	1.75 ± 0.05 mm
Recommended printing temperature	230–250 °C
Recommended printing speed	30–90 mm/s
Extrusion temperature (°C)	190–210
Heated bed temperature (°C)	80
Density (g/cm^3)	1.04

2.2. Experimental Design

According to the literature, the mechanical characteristics of FDM-produced components are highly impacted by process parameters. It was also vital to examine the

combined effects of FDM parameters on the mechanical characteristics of the produced components. As a result, five crucial process parameters were chosen as inputs for this research: raster angle, orientation angle, air gap, raster width, and layer height with three levels. The values of each element were adjusted according to machine manufacturer recommendations. Table 3 lists the process parameters and their ranges that were explored during this study. The other parameters were retained at their default settings. A total of 46 experiments were utilized, based on the Box–Behnken response surface experimental design, which depends on the number of input variables, and their levels as shown in Table 4.

Table 3. Process parameters and their range for experiments.

S.No.	Process Parameters	Units	Levels		
			Low (−1)	Medium (0)	High (+1)
1	Raster angle		0	30	60
2	Printing orientation		0	30	60
3	Air gap	mm	0	0.003	0.006
4	Raster width	mm	0.4064	0.4464	0.4864
5	Layer height	mm	0.14	0.185	0.23

Table 4. Box—Behnken response surface experimental design matrix and measured responses.

Run Order	Std Order	Raster Angle (°)	Printing Orientation (°)	Air Gap (mm)	Raster Width (mm)	Layer Height (mm)	Tensile Strength (MPa)
8	1	0	0	0.003	0.4464	0.185	27.835
2	2	60	0	0.003	0.4464	0.185	15.585
34	3	0	60	0.003	0.4464	0.185	10.248
30	4	60	60	0.003	0.4464	0.185	16.198
45	5	30	30	0	0.4064	0.185	20.608
13	6	30	30	0.006	0.4064	0.185	13.283
1	7	30	30	0	0.4864	0.185	19.983
14	8	30	30	0.006	0.4864	0.185	19.758
31	9	30	0	0.003	0.4464	0.14	19.642
17	10	30	60	0.003	0.4464	0.14	10.854
40	11	30	0	0.003	0.4464	0.23	23.129
10	12	30	60	0.003	0.4464	0.23	14.942
16	13	0	30	0	0.4464	0.185	23.804
15	14	60	30	0	0.4464	0.185	16.654
46	15	0	30	0.006	0.4464	0.185	16.029
9	16	60	30	0.006	0.4464	0.185	16.879
33	17	30	30	0.003	0.4064	0.14	12.835
41	18	30	30	0.003	0.4864	0.14	17.810
37	19	30	30	0.003	0.4064	0.23	18.673
43	20	30	30	0.003	0.4864	0.23	19.548
22	21	30	0	0	0.4464	0.185	29.415
27	22	30	60	0	0.4464	0.185	11.027
38	23	30	0	0.006	0.4464	0.185	15.740
18	24	30	60	0.006	0.4464	0.185	17.152
19	25	0	30	0.003	0.4064	0.185	19.639
4	26	60	30	0.003	0.4064	0.185	12.592
21	27	0	30	0.003	0.4864	0.185	18.604
36	28	60	30	0.003	0.4864	0.185	19.404

29	29	30	30	0	0.4464	0.14	19.285
12	30	30	30	0.006	0.4464	0.14	12.960
42	31	30	30	0	0.4464	0.23	20.523
7	32	30	30	0.006	0.4464	0.23	19.298
11	33	0	30	0.003	0.4464	0.14	17.006
20	34	60	30	0.003	0.4464	0.14	13.506
3	35	0	30	0.003	0.4464	0.23	20.443
25	36	60	30	0.003	0.4464	0.23	17.644
23	37	30	0	0.003	0.4064	0.185	18.239
44	38	30	60	0.003	0.4064	0.185	13.902
5	39	30	0	0.003	0.4864	0.185	25.314
28	40	30	60	0.003	0.4864	0.185	12.677
6	41	30	30	0.003	0.4464	0.185	15.210
24	42	30	30	0.003	0.4464	0.185	15.211
35	43	30	30	0.003	0.4464	0.185	15.200
32	44	30	30	0.003	0.4464	0.185	15.220
26	45	30	30	0.003	0.4464	0.185	15.210
39	46	30	30	0.003	0.4464	0.185	15.200

2.3. Specimen Fabrication

The test specimen was 3D modeled using CATIA V5 software, as per the criteria. The stereo lithography (STL) format is used to save the CAD file, which is then transferred to the slicer for separation into the needed number of layers. Using flash print slicing software, the printing settings are also included. The slicer then transforms the STL file to a G-code file, which the printers use to begin layer-by-layer fabrication of the specimen. The tensile test specimens were made according to the American Society for Testing and Materials (ASTM) D638-I standard. The length, width, and thickness of ASTM D638-I are 165 × 13 × 3.2 mm as shown in Figure 1.

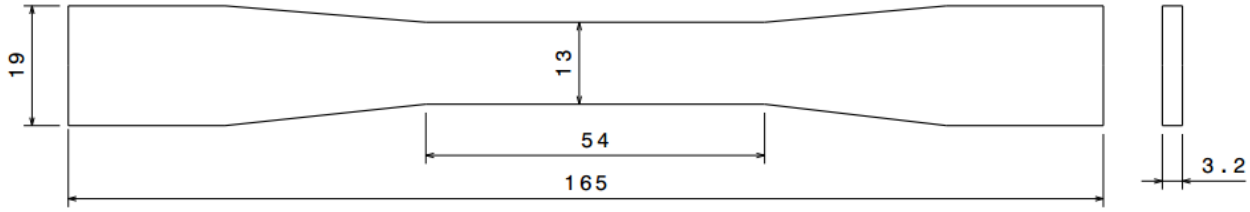

Figure 1. The ASTM D638-I tensile test sample**.**

2.4. Experimental Procedure

The universal testing equipment was used to assess the tensile strength of ABS specimens that had been conditioned according to the ASTM D638 standard as shown in Figure 2. The top grip moved at a continuous rate of 2.5 mm/min with a maximum load of 100 KN and a 5 Hz signal sampling rate. The built-in program recorded the elongation and force load data. When the specimen elongates or fractures by more than 2.5 percent, the ASTM D638 test is completed. The tensile strength is calculated from the breaking load and is divided by the initial cross section area according to Equation (1). In this study, 46 experimental tests were conducted with two replications, and no differences between the two replications were observed (presented in Table 4).

$$\boldsymbol{Tensile\ strength\ (UTS)} = \frac{\boldsymbol{Breaking\ load(Pf)}}{\boldsymbol{(orignal\ cross\ sectional\ area(Ao)}} \quad (1)$$

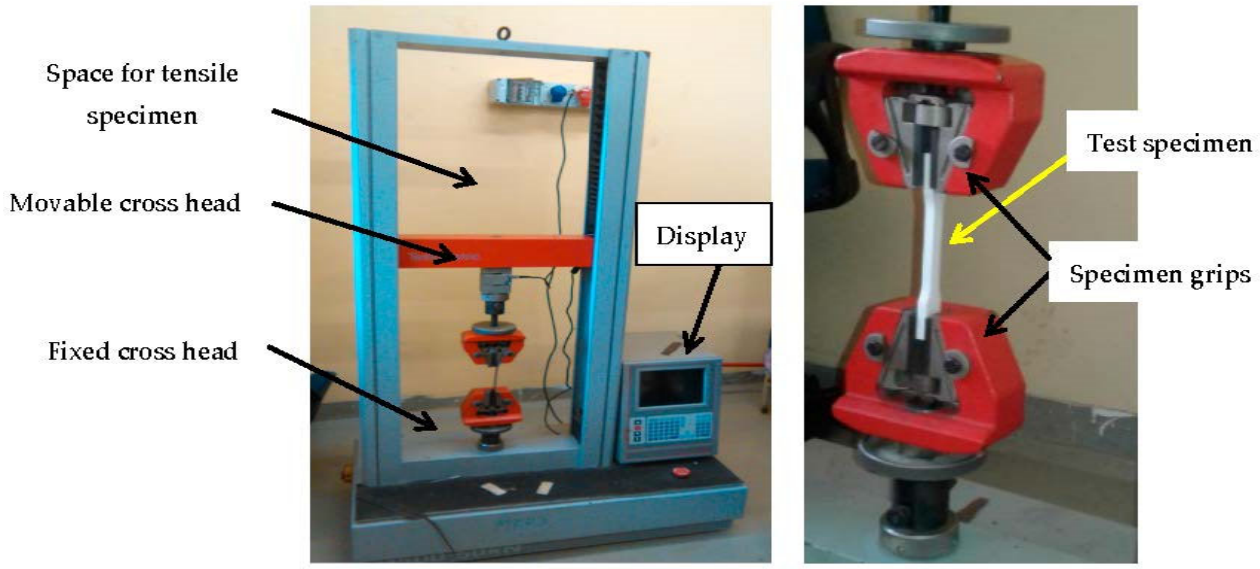

Figure 2. Universal testing machine with testing specimen.

2.5. Adaptive Neuro-Fuzzy Modeling

The architecture and learning approach of neuro-fuzzy techniques (also known as an adaptive neuro-fuzzy model) was initially developed by Jang [29]. ANFIS is a powerful approach that integrates neural networks' optimization and learning skills with the reasoning capabilities of fuzzy logic linguistic IF–THEN rules, which are made up of membership functions (MF). It combines the benefits of fuzzy logic with artificial neural networks. The ANFIS model is especially beneficial when data are inconsistent or nonlinear and established methodologies fail or are too difficult to apply with greater precision [30–34].

In this study, the ANFIS model was stimulated using the fuzzy inference system concept as a five-layered neural network. The parameters of the ANFIS model are listed in Table 5. MATLAB R2019a software was used to run the simulations. The first and last levels of the ANFIS structure and layer indicate the respective input variables (raster angle, orientation angle, air gap, raster width, and layer height) and output variable (tensile strength), as shown in Figure 3. In the second layer, the model employed first-Sugeno inference systems, which turn input parameters into membership values using membership functions called fuzzification. The model output is then deduced using a set of logical rules in the third layer.

Table 5. Details of the ANFIS model used in this study.

ANFIS Information	Takagi–Sugeno–Kang
Number of MFs	3 3 3 3 3
MF type (Input)	Trapmf
Output MF types	Constant
Optimization method	Hybrid
Error tolerance	1×10^{-7}
Epochs	100
FIS generation	Grid partitioning (GP)
Data points	32
Number of fuzzy rules	243

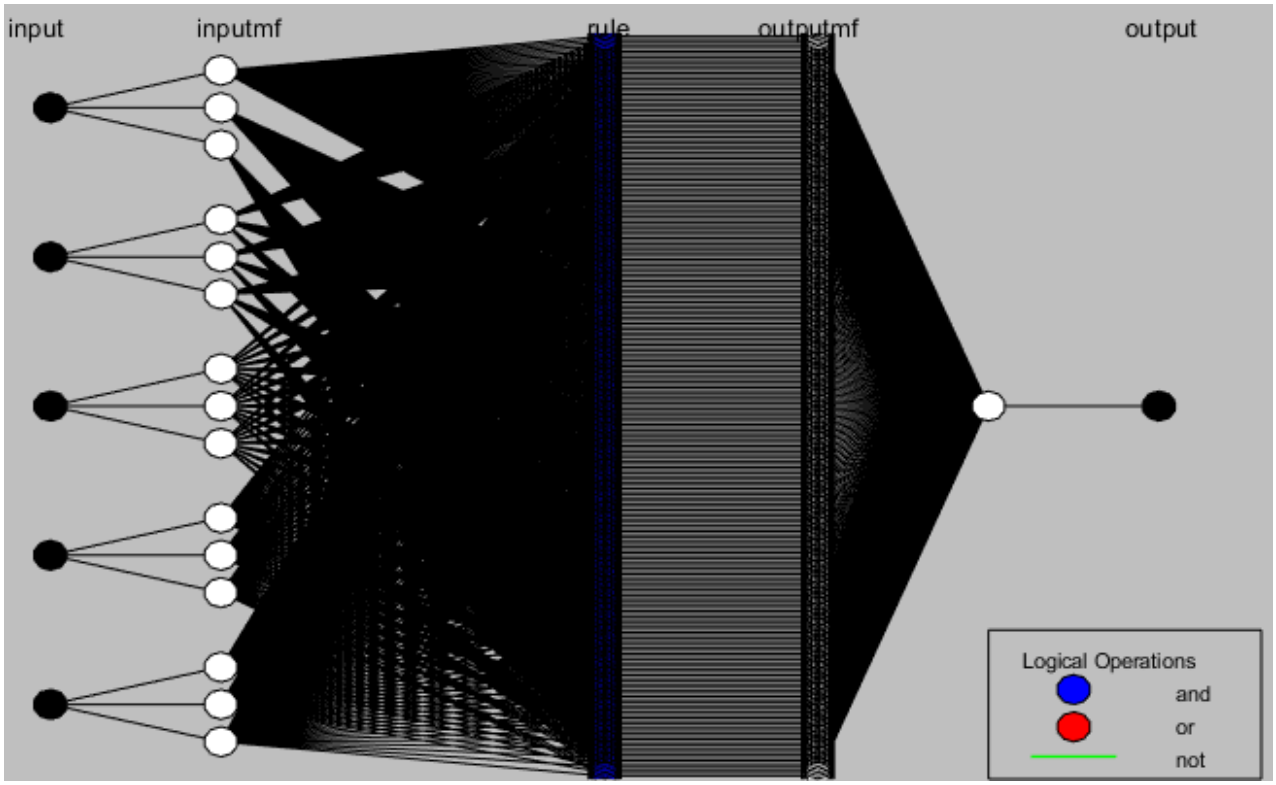

Figure 3. ANFIS multilayer architecture.

2.6. Artificial Neural Network Modeling

Artificial neural networks (ANNs) are computational models based on the organic neural networks in the human brain. An ANN is used to mimic non-linear situations and predict output values using training data. Input and output layers, as well as multiple hidden layer neurons, comprise an ANN structural network [35–37]. ANN uses samples of data rather than the whole data set available in the system for quick prediction, saving money and time. ANNs can be easily replaced by existing data analysis systems [38].

The ANN model was used to train and assess the 3D printing data models. An input layer with five inputs, a hidden layer with feed-forward conditions added, and one output layer were created using MATLAB as shown in Figure 4. The experimental data from Table 4 were used to train the network. The parameters of the ANN model are listed in Table 6. Figure 4 depicts the ANN architecture and learning variables used in this investigation.

Table 6. Learning parameters designated for the ANN.

Type of Network	Feed-Forward Neural Network
Training function	Train Levenberg–Marquardt (LM) algorithm
Adaption Learning function	LEARNGD (Gradient descent)
Performance function	Mean square error
Network topology	5-50-1-1
Transfer function	TANSIG
Number of Hidden Layers	1
Number of Hidden Neurons	50
Training method	Back-propagation
Number of Epochs	1000

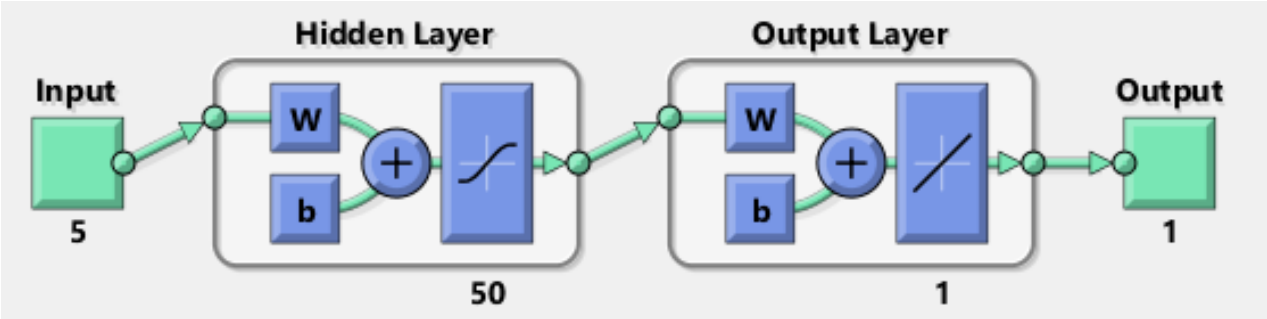

Figure 4. Structure of the neural network.

3. Results and Discussion

3.1. Effect of Process Parameters on Tensile Strength

Analysis of variance (ANOVA) was used to examine the results for tensile characteristics in order to explore the major factors that influence the quality measures. Factors with a very modest probability (Prob. > F-value less than 0.05) are considered significant in the ANOVA table, whereas factors with a probability (Prob. > F-value) larger than 0.1 are considered inconsequential. Furthermore, larger F-values and lower p-values have a greater impact on the performance characteristics derived from designed process parameters. Table 7 shows the ANOVA of each process parameter with respect to the ultimate tensile strength of ABS parts, where A is the raster angle, B is the printing orientation, C is the air gap, D is the raster width, and E is the layer height. According to the ANOVA table (Table 7), printing orientation, layer height, raster angle, and layer height combinations, the air gap and layer height combinations are insignificant factors that impact the ultimate tensile strength of ABS components. Since the p-values of the raster angle, printing orientation, raster width, air gap, and their combinations are less than 0.05, they have a significant impact on the UTS of ABS-printed parts.

Table 7. ANOVA for ultimate tensile strength of ABS parts.

Source	DF	Adj. SS	Adj. MS	F-Value	*p*-Value	
Regression	20	772.083	38.6042	133.88	0.000	
A	1	30.224	30.2237	104.82	0.000	Significant
B	1	1.175	1.175	4.07	0.054	Insignificant
C	1	39.473	39.4735	136.89	0.000	Significant
D	1	8.424	8.4238	29.21	0.000	Significant
E	1	0.643	0.643	2.23	0.148	Insignificant
A*A	1	11.292	11.2923	39.16	0.000	Significant
B*B	1	11.127	11.1274	38.59	0.000	Significant
C*C	1	35.055	35.0547	121.57	0.000	Significant
D*D	1	12.655	12.6547	43.89	0.000	Significant
E*E	1	5.761	5.7614	19.98	0.000	Significant
A*B	1	82.81	82.81	287.19	0.000	Significant
A*C	1	16	16	55.49	0.000	Significant
A*D	1	15.603	15.6025	54.11	0.000	Significant
A*E	1	0.122	0.1225	0.42	0.52	Insignificant
B*C	1	98.01	98.01	339.9	0.000	Significant
B*D	1	17.222	17.2225	59.73	0.000	Significant
B*E	1	0.09	0.09	0.31	0.581	Insignificant
C*D	1	12.603	12.6025	43.71	0.000	Significant
C*E	1	6.503	6.5025	22.55	0.000	Significant

D*E	1	4.203	4.2025	14.57	0.001	Significant
Error	25	7.209	0.2883			
Lack-of-Fit	20	7.209	0.3604			
Pure Error	5	0.000	0.0001			
Total	45	779.292				

Figure 5 illustrates the main effects plot for UTS, which shows how UTS vary depending on the inputs. The mean UTS value started to decrease with increasing raster angle, printing orientation, and air gap, as shown in this main effect graph. The UTS also improved as the raster width and layer height started escalating. According to the main effects plot shown in Figure 5, a lower raster angle, printing orientation, air gap, and higher raster width and layer height would result in enhanced UTS.

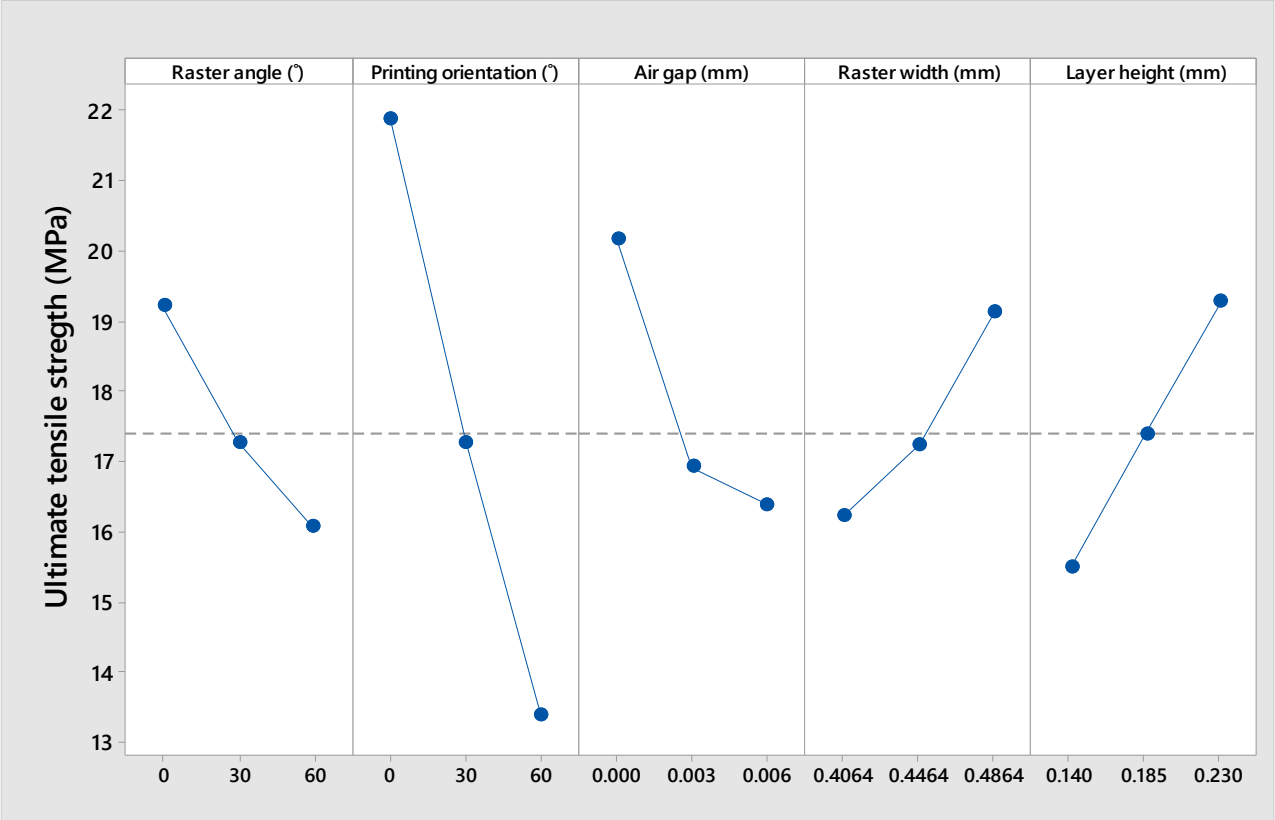

Figure 5. Main effect plots of UTS for means with all process parameters.

Figures 6–8 show 3D and contour graphs depicting the impact of both of the input factors on the ultimate tensile strength. In these figures, blue-colored zones represent very low and low levels, green zones reflect low–medium, medium, and high–medium levels, while yellow zones represent high and very high volumes. The effect of raster angle (input 1) and printing orientation (input 2) on the UTS is shown in Figure 6. It shows that lower raster angles and printing orientation led to increased UTS values. Figure 7 depicts the influence of the air gap (input 3) and raster width (input 4) on the UTS in a similar way, showing that reduced air gaps and larger raster widths yielded higher UTS values. These interaction graphs also show that raster width had a moderate influence on UTS. The effects of raster width (input 4) and layer height (input 5) on the UTS are also shown in Figure 8. Higher UTS values were achieved when the raster width and layer height were increased.

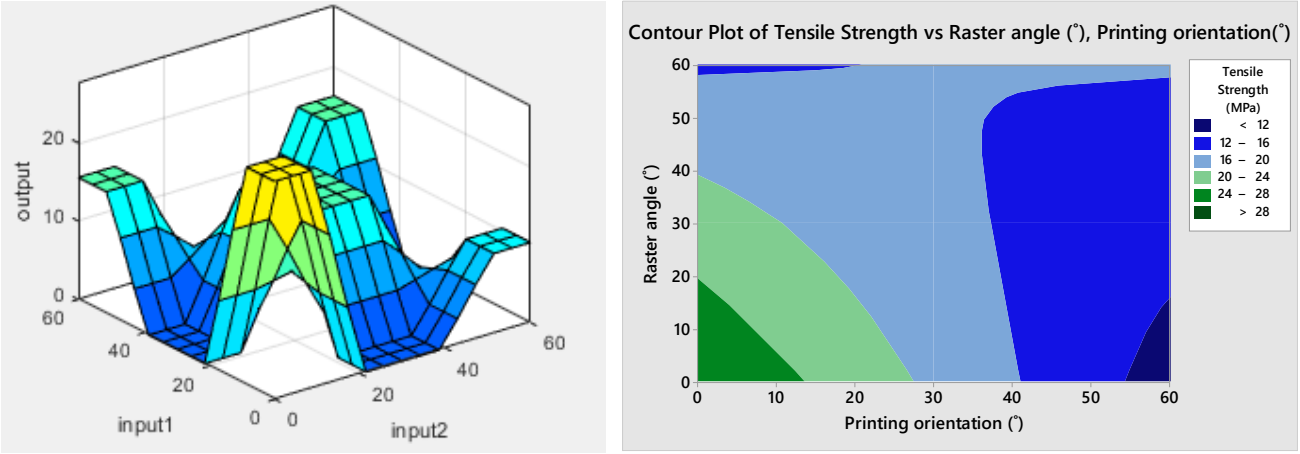

(**a**) (**b**)

Figure 6. 3D plot (**a**) and controur plot (**b**) of tensile strength vs. raster angle and printing orientation.

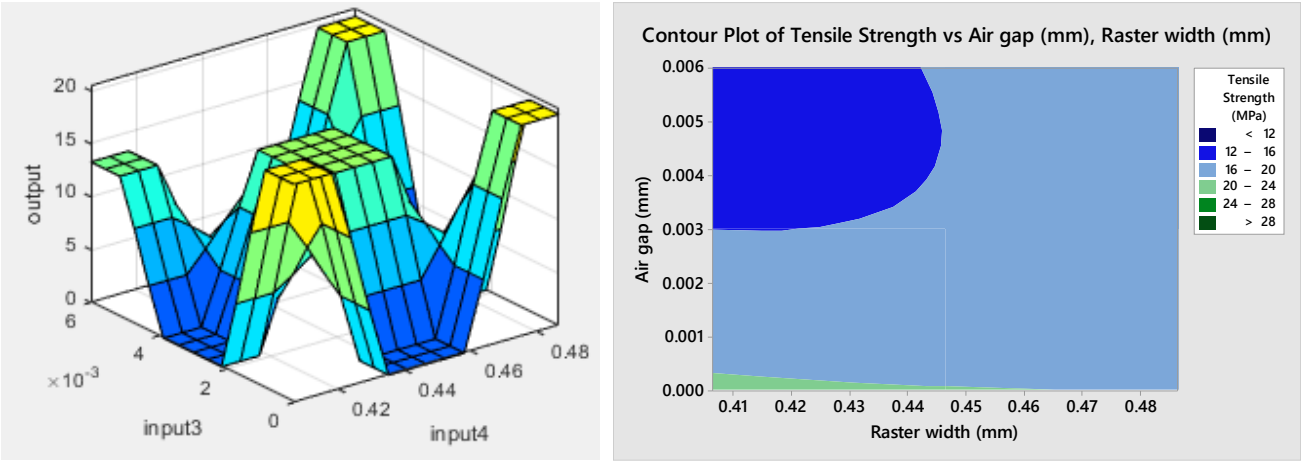

(**a**) (**b**)

Figure 7. 3D plot (**a**) and contour plot (**b**) of tensile strength vs. air gap and raster width.

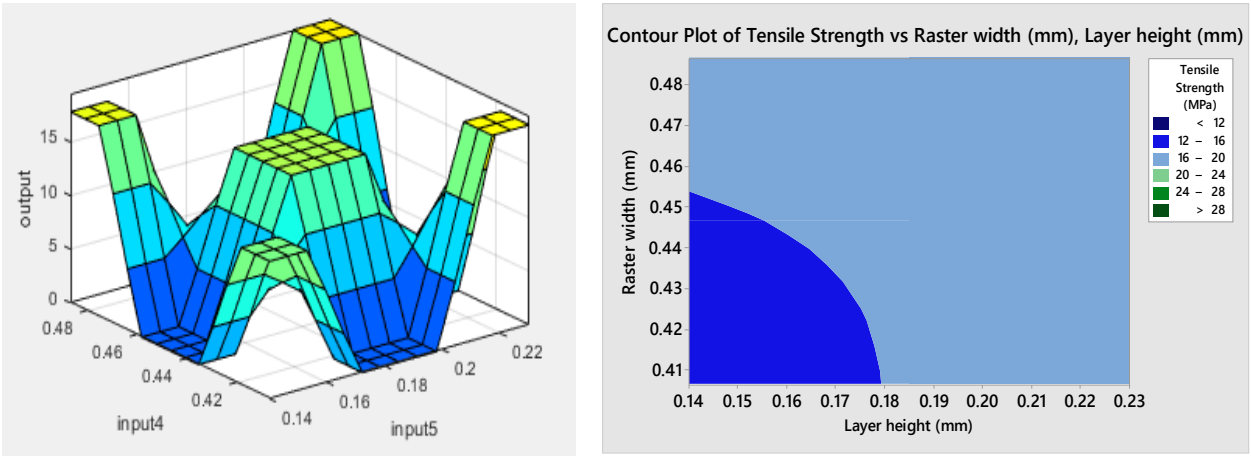

(**a**) (**b**)

Figure 8. 3D plot (**a**) and contour plot (**b**) of tensile strength vs. raster width and layer height.

3.2. Results of ANFIS Modeling

For the prediction of the tensile strength of ABS-printed components using FDM, an ANFIS model was created utilizing the data gained from experimental measurements. A number of factors must be adjusted to identify the best model architecture for the ANFIS model. To develop a robust model with sufficient predictive performance, parameters such as the number of rules, type, and number of MFs, and logical operators must be modified. Based on the data in Table 4, the results of the proposed ANFIS model were obtained using the MATLAB R2019a program, and the predicted data are shown in Table 6. Figure 9 shows the two hundred and forty-four IF–THEN membership functions (MF) rules used to train the ANFIS model in this study. It also illustrates that the predicted results of UTS were 15.2 MPa when the raster angle (input 1) was 30 degrees, the printing orientation (input 2) was 30 degrees, the air gap (input 3) was 0.4466 mm, the raster width (input 4) was 0.185 mm, and the layer height (input 5) was 100 mm/s. The suggested model was valid after evaluating the checking data with the derived FIS model, with a minimal checking RMSE of 0.002500, which is less than 0.3080 % error. As shown in Figure 10, the R^2 value between predicted and targeted values for ANFIS tensile strength demonstrated a high level of accuracy, with $R^2 = 0.9999$, indicating that the model is valid.

Figure 9. Representation of rules for the generated FIS.

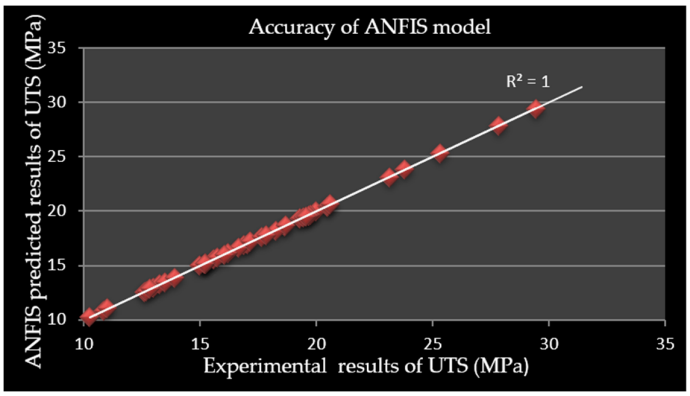

Figure 10. Regression results of the ANFIS model.

3.3. Results of ANN Modeling

When the error, or the difference between the expected and predicted output, is less than a defined upper bound, or when the number of epochs exceeds a specified threshold, the ANN stops training. A score near 1 implies a strong connection, while a value close to 0 shows a random relation. Figure 11 illustrates the 12-iteration regression graphs developed by artificial neural networks. The regression plots obtained reveal that for training, testing, validation, and total data, the values were 0.98228, 0.85711, 0.92749, and 0.917, respectively, suggesting the best fitness after repeated training. This indicates that the ANN model's anticipated outcomes appear to be in line with the experimental data. The ANN model worked adequately, as shown in Table 8, with an average percentage error of 1.6437 from the experimental results, demonstrating its potential for future usage.

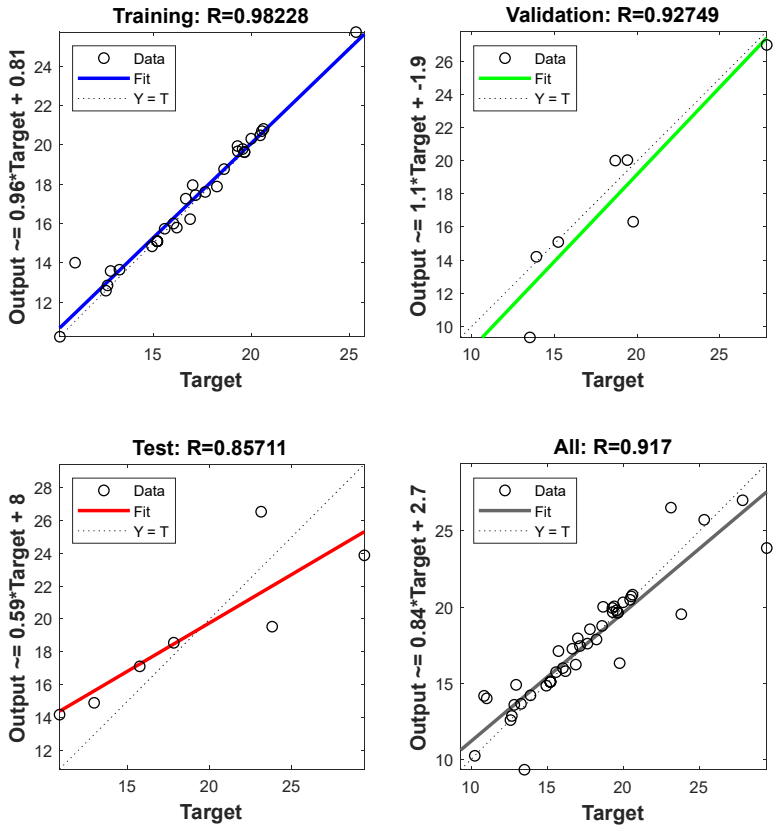

Figure 11. Regression plots for ultimate tensile strength obtained using the ANN model.

Table 8. Comparative evaluation of predictive models.

Exp. Trials	Experimental Results of UTS	ANFIS Model		ANN Model	
		Predicted Results	% Errors	Predicted Results	% Errors
1.	19.983	19.985	−0.0100	20.309	−1.6314
2.	15.585	15.587	−0.0128	15.732	−0.9432
3.	20.443	20.442	0.0049	20.481	−0.1859
4.	12.592	12.593	−0.0079	12.578	0.1112
5.	25.314	25.317	−0.0119	25.735	−1.6631
6.	15.210	15.207	0.0197	15.094	0.7627
7.	19.298	19.292	0.0311	19.672	−1.9380
8.	27.835	27.839	−0.0144	27.017	2.9387
9.	16.879	16.880	−0.0059	16.221	3.8983
10.	14.942	14.941	0.0067	14.835	0.7161
11.	17.006	17.009	−0.0176	17.756	−4.4102
12.	12.960	12.961	−0.0077	13.294	−2.5772
13.	13.283	13.287	−0.0301	13.647	−2.7403
14.	19.758	19.761	−0.0152	18.8662	4.5136
15.	16.654	16.652	0.0120	17.263	−3.6568
16.	23.804	23.812	−0.0336	23.3201	2.0329
17.	10.854	10.860	−0.0553	11.1657	−2.8718
18.	17.152	17.150	0.0117	17.443	−1.6966
19.	19.639	19.634	0.0255	19.9011	−1.3346
20.	13.506	13.501	0.0370	13.3181	1.3912
21.	18.604	18.603	0.0054	18.764	−0.8600
22.	29.415	29.414	0.0034	28.8888	1.7889
23.	18.239	18.243	−0.0219	17.876	1.9902
24.	15.211	15.204	0.0460	15.094	0.7692
25.	17.644	17.643	0.0057	17.602	0.2380
26.	15.210	15.203	0.0460	15.094	0.7627
27.	11.027	11.026	0.0091	10.7033	2.9355
28.	12.677	12.676	0.0079	12.851	−1.3726
29.	19.285	19.281	0.0207	19.938	−3.3861
30.	16.198	16.196	0.0123	15.789	2.5250
31.	19.642	19.641	0.0051	19.645	−0.0153
32.	15.220	15.203	0.1117	15.094	0.8279
33.	12.835	12.834	0.0078	12.587	1.9322
34.	10.248	10.246	0.0195	10.236	0.1171
35.	15.200	15.212	−0.0789	15.094	0.6974
36.	19.404	19.405	−0.0052	20.048	−3.3189
37.	18.673	18.672	0.0054	19.1365	−2.4822
38.	15.740	15.739	0.0064	16.111	−2.3571
39.	15.200	15.210	−0.0658	15.094	0.6974
40.	23.129	23.128	0.0043	23.0753	0.2322
41.	17.810	17.811	−0.0056	18.549	−4.1494
42.	20.523	20.522	0.0049	20.698	−0.8527
43.	19.548	19.551	−0.0153	19.785	−1.2124
44.	13.902	13.901	0.0072	14.204	−2.1723
45.	20.608	20.607	0.0049	20.812	−0.9899
46.	16.029	16.026	0.0187	15.995	0.2121
Average percentage error			0.0163		1.6437

3.4. Comparative Evaluation of the Predictive Models

To compare the ANFIS and ANN, the predictive results and the experimental results of UTS were analyzed by the average percentage error of the responses. The percentages of absolute errors for ANFIS and ANN were computed individually by comparing the predicted values with the test results using Equation (2)**Error! Reference source not found.**. The average percentage error of the ANFIS model was 0.0163 %, and that of the ANN model was 1.6437 %, as shown in Table 8. This demonstrates that the ANFIS model is the most accurate or best-predicting model technique.

$$\%\ \boldsymbol{Absolute\ error} = \frac{\boldsymbol{Actual - predicted}}{\boldsymbol{Actual}} \times \mathbf{100} \quad (2)$$

3.5. Validation of the Models

In order to validate the relative performances of the ANFIS and ANN models, the validation parameters had different values of process parameters for eight new validation specimens. The validation parameters had the raster angle, printing orientation, air gap, raster width, and layer height as shown in Table 9. New specimens were fabricated and tested for tensile strength using the above parameters, and the percentage in deviation was computed using the means of prediction under ANFIS and ANN in MINITAB 2019a. When comparing the actual and predicted outcomes using the ANFIS and ANN approaches, the validation parameter yielded the percentage error as 0.166 and 0.767, respectively. Hence, the ANFIS model's accuracy ranges from 1 to 2%, whereas the ANN model's accuracy ranges from 1 to 5%.

Table 9. Process parameters for validation.

Run Order	Raster Angle (°)	Printing Orientation (°)	Air Gap (mm)	Raster Width (mm)	Layer Height (mm)	Exp. results of UTS (MPa)	ANFIS Model		ANN Model	
							Predicted Results (MPa)	% Errors	Predicted Results (MPa)	% Errors
1	15	15	0.002	0.4264	0.17	9.690	9.689	0.011	9.558	1.363
2	15	15	0.002	0.4664	0.20	10.500	10.508	−0.072	10.482	0.175
3	15	45	0.004	0.4264	0.17	7.043	7.040	0.045	7.040	0.047
4	15	45	0.004	0.4664	0.20	7.012	7.010	0.034	7.017	−0.063
5	45	15	0.004	0.4264	0.20	7.500	7.581	−1.079	7.173	4.361
6	45	15	0.004	0.4664	0.17	8.931	8.930	0.006	8.932	−0.019
7	45	45	0.002	0.4264	0.20	7.052	7.049	0.048	7.051	0.024
8	45	45	0.002	0.4664	0.17	7.541	7.538	0.040	7.522	0.248

4. Conclusions

This research proposes experimental analysis and the use of adaptive neuro-fuzzy methods and artificial neural networks to forecast the tensile strength for ABS components manufactured using fused deposition modeling. All of the investigations were carried out using a 46 Box–Behnken response surface design to alter the input parameters at different levels. Analysis of variance, main effect plots, 3D, and contour plots were used to investigate the link between input parameters and output results. The experimental outcomes were used to train and evaluate the models that were developed. The MATLAB R2019a fuzzy toolbox and neural toolbox were used to create the neuro-fuzzy system and artificial neural network, respectively. The ability of the models to forecast was tested using percentage errors. The study revealed that layer height, raster angle and layer height combinations, and air gap and layer height combinations were insignificant factors that impacted the ultimate tensile strength of ABS components. Since the p-values of the raster angle, printing orientation, raster width, air gap, and their

combinations were less than 0.05, they had a significant impact on the ABS-printed components' tensile strength. The UTS started to decrease with increasing raster angle, printing orientation, and air gap. The UTS also improved as the raster width and layer height started increasing. Enhanced mechanical strength may be achieved by using a lower raster angle, printing orientation, air gap, and larger raster width and layer height. The ANFIS and ANN models can accurately predict tensile strength with average percentage errors of 0.0163 and 1.6437, respectively. The ANFIS model's accuracy ranges from 1 to 2%, whereas the ANN model's accuracy ranges from 1 to 5%. This shows the predicted and experimental data are in good agreement. The arithmetical value indices of the ANFIS model indicated a better predictive performance than that of the ANN model.

Author Contributions: Conceptualization, A.D.T., and H.B.M.; methodology, A.D.T.; software, A.D.T.; validation, A.D.T.; formal analysis, A.D.T. and H.B.M.; investigation, A.D.T. and H.B.M.; resources, A.D.T. and H.G.L.; data curation, A.D.T. and H.G.L.; writing—original draft preparation, A.D.T.; writing—review and editing, A.D.T and H.G.L.; visualization, H.G.L.; supervision, H.G.L.; project administration, H.B.M.; funding acquisition, H.G.L. All authors have read and agreed to the published version of the manuscript.

Funding: This research received no external funding.

Institutional Review Board Statement: Not applicable.

Informed Consent Statement: Not applicable.

Data Availability Statement: Not applicable.

Conflicts of Interest: The authors declare no conflict of interest.

References

1. Sheoran, A.J.; Kumar, H. Fused Deposition modeling process parameters optimization and effect on mechanical properties and part quality : Review and reflection on present research. *Mater. Today Proc.* **2019**, *10*, 14.
2. Amelia, N.; Ferliadi, F.; Christa, A.; Gunawan, F.E.; Asrol, M. Experimental Investigation on Influence of Infill Density on Tensile Mechanical Properties of Different FDM 3D Printed Materials. *TEM J.* **2021**, *10*, 1195–1201.
3. Wankhede, V.; Jagetiya, D.; Joshi, A.; Chaudhari, R. Experimental investigation of FDM process parameters using Taguchi analysis. *Mater. Today Proc.* **2019**, *27*, 2117–2120.
4. Scallan, P. Comparative Study of the Sensitivity of PLA, ABS, PEEK, and PETG's Mechanical Properties to FDM Printing Process Parameters. *Crystals* **2021**, *11*, 219–250.
5. Milovanović, A.; Sedmak, A.; Grbović, A.; Golubović, Z.; Mladenović, G.; Čolića, K.; Milošević, M. Comparative analysis of printing parameters effect on mechanical properties of natural PLA and advanced PLA-X material. *Procedia Struct. Integr.* **2020**, *28*, 1963–1968.
6. Onwubolu, G.C.; Rayegani, F. Characterization and Optimization of Mechanical Properties of ABS Parts Manufactured by the Fused Deposition Modelling Process. *Hindawi* **2014**, *2014*, 1–13.
7. Mamo, H.B.; Tura, A.D.; Santhosh, A.J.; Ashok, N.; Rao, D.K. Modeling and analysis of flexural strength with fuzzy logic technique for a fused deposition modeling ABS components. *Mater. Today Proc.* **2022**, *57*, 768–774.
8. Wang, S.; Ma, Y.; Deng, Z.; Zhang, S.; Cai, J. Effects of fused deposition modeling process parameters on tensile, dynamic mechanical properties of 3D printed polylactic acid materials. *Polym. Test.* **2020**, *86*, 106483.
9. Lluch-Cerezo, J.; Benavente, R.; Meseguer, M.D.; Gutiérrez, S.C. Study of samples geometry to analyze mechanical properties in Fused Deposition Modeling process (FDM). *Procedia Manuf.* **2019**, *41*, 890–897.
10. Zhou, X.; Hsieh, S.; Ting, C. Modelling and estimation of tensile behaviour of polylactic acid parts manufactured by fused deposition modelling using finite element analysis and knowledge-based library. *Virtual Phys. Prototyp.* **2018**, *13*, 177–190.
11. Gebisa, A.W.; Lemu, H.G. Influence of 3D printing FDM process parameters on tensile property of ultem 9085. *Procedia Manuf.* **2019**, *30*, 331–338.
12. Byberg, K.I.; Gebisa, A.W.; Lemu, H.G. Mechanical properties of ULTEM 9085 material processed by fused deposition modeling. *Polym. Test.* **2018**, *72*, 335–347.
13. Motaparti, K.P.; Taylor, G.; Leu, M.C.; Chandrashekhara, K.; Castle, J.; Matlack, M. Experimental investigation of effects of build parameters on flexural properties in fused deposition modelling parts. *Virtual Phys. Prototyp.* **2017**, *12*, 207–220.
14. Gebisa, A.W.; Lemu, H.G. Investigating Effects of Fused-Deposition Modeling (FDM) Processing Parameters on Flexural Properties of ULTEM 9085 using Designed Experiment. *Materials* **2018**, *11*, 500. https://doi.org/10.3390/ma11040500.

15. Christiyan, K.G.J.; Chandrasekhar, U.; Venkateswarlu, K. A study on the influence of process parameters on the Mechanical Properties of 3D printed ABS composite. *IOP Conf. Ser. Mater. Sci. Eng.* **2016**, *114*, 12109.
16. Hsueh, M.-H.; Lai, C.-J.; Wang, S.-H.; Zeng, Y.-S.; Hsieh, C.-H.; Pan, C.-Y.; Huang, W.-C. Effect of Printing Parameters on the Thermal and Mechanical Properties of 3D-Printed PLA and PETG, Using Fused Deposition Modeling. *Polymers* **2021**, *13*, 1758.
17. Enemuoh, E.U.; Duginski, S.; Feyen, C.; Menta, V.G. Effect of Process Parameters on Energy Consumption, Physical, and Mechanical Properties of Fused Deposition Modeling. *Polymers* **2021**, *13*, 2406.
18. Hsueh, M.-H.; Lai, C.-J.; Liu, K.-Y.; Chung, C.-F.; Wang, S.-H.; Pan, C.-Y.; Huang, W.-C.; Hsieh, C.-H.; Zeng, Y.-S. Effects of Printing Temperature and Filling Percentage on the Mechanical Behavior of Fused Deposition Molding Technology Components for 3D Printing. *Polymers* **2021**, *13*, 2910.
19. Patil, C.; Sonawane, P.D.; Naik, M.; Thakur, D.G. Finite element analysis of flexural test of additively manufactured components fabricated by fused deposition modelling. In *AIP Conf. Proc.* **2020**, *2311*, 070026. https://doi.org/10.1063/5.0034306.
20. Pazhamannil, R.V.; Govindan, P.S.P. Prediction of the tensile strength of polylactic acid fused deposition models using artificial neural network technique. *Mater. Today Proc.* **2020**, *199*, 9187–9193.
21. Rayegani, F.; Onwubolu, G.C. Fused deposition modelling (FDM) process parameter prediction and optimization using group method for data handling (GMDH) and differential evolution (DE). *Int. J. Adv. Manuf. Technol.* **2014**, *2*, 509–519.
22. Srinivasan, R.; Pridhar, T.; Ramprasath, L.S.; Charan, N.S.; Ruban, W. Proceedings Prediction of tensile strength in FDM printed ABS parts using response surface methodology (RSM). *Mater. Today Proc.* **2020**, *3*, 788.
23. Vishwakarma, S.K.; Pandey, P.; Gupta, N.K. Characterization of ABS Material: A Review. *J. Res. Mech. Eng.* **2017**, *3*, 13–16.
24. Harris, M.; Potgieter, J.; Ray, S.; Archer, R.; Arif, K.M. Acrylonitrile butadiene styrene and polypropylene blend with enhanced thermal and mechanical properties for fused filament fabrication. *Materials* **2019**, *12*, 24.
25. Rutkowski, J.V.; Levin, B.C. Acrylonitrile–butadiene–styrene copolymers (ABS): Pyrolysis and combustion products and their toxicity—a review of the literature. *Fire Mater.* **1986**, *10*, 93–105.
26. Nguyen, H.T.; Crittenden, K.; Weiss, L.; Bardaweel, H. Experimental Modal Analysis and Characterization of Additively Manufactured Polymers. *Polymers* **2022**, *14*, 2071.
27. Akessa, A.D.; Lemu, H.G.; Gebisa, A.W. Mechanical Property Characterization of Additive Manufactured ABS Material Using Design of Experiment Approach. In Proceedings of the ASME 2017 International Mechanical Engineering Congress and Exposition, Volume 14: Emerging Technologies; Materials: Genetics to Structures, Safety Engineering and Risk Analysis, Tampa, FL, USA, 3–9 November 2017.
28. Croccolo, D.; De Agostinis, M.; Olmi, G. Experimental characterization and analytical modelling of the mechanical behaviour of fused deposition processed parts made of ABS-M30. *Comput. Mater. Sci.* **2013**, *79*, 506–518.
29. Zadeth, L.A. Fuzzy sets as a basis for a theory of possibility. *Fuzzy Sets Syst.* **1999**, *148*, 9–34.
30. Sarkar, J.; Prottoy, Z.H.; Bari, M.T.; al Faruque, M.A. Comparison Of Anfis And Ann Modeling For Predicting The Water Absorption Behavior Of Polyurethane Treated Polyester Fabric. *Heliyon* **2021**, *7*, e08000.
31. Ghorbani, B.; Arulrajah, A.; Narsilio, G.; Horpibulsuk, S.; Leong, M. Resilient moduli of demolition wastes in geothermal pavements: Experimental testing and ANFIS modelling. *Transp. Geotech.* **2021**, *29*, 100592.
32. Saleh, B.; Maher, I.; Abdelrhman, Y.; Heshmat, M.; Abdelaal, O. Adaptive Neuro-Fuzzy Inference System for Modelling the Effect of Slurry Impacts on PLA Material Processed by FDM. *Polymers* **2021**, *13*, 118.
33. Nafees, A.; Javed, M.F.; Khan, S.; Nazir, K.; Farooq, F.; Aslam, F.; Musarat, M.A.; Vatin, N.I. Predictive Modeling of Mechanical Properties of Silica Fume-Based Green Concrete Using Artificial Intelligence Approaches: MLPNN, ANFIS, and GEP. *Materials* **2021**, *14*, 7531.
34. Zhu, H.; Zhu, L.; Sun, Z.; Khan, A. Machine learning based simulation of an anti-cancer drug (busulfan) solubility in supercritical carbon dioxide: ANFIS model and experimental validation. *J. Mol. Liq.* **2021**, *338*, 116731.
35. Santhosh, A.J.; Tura, A.D.; Jiregna, I.T.; Gemechu, W.F.; Ashok, N.; Ponnusamy, M. Optimization of CNC turning parameters using face centred CCD approach in RSM and ANN-genetic algorithm for AISI 4340 alloy steel. *Results Eng.* **2021**, *11*, 00251.
36. Tura, A.D.; Mamo, H.B.; Jelila, Y.D.; Lemu, H.G. Experimental investigation and ANN prediction for part quality improvement of fused deposition modeling parts. *IOP Conf. Ser. Mater. Sci. Eng.* **2021**, *1201*, 012031.
37. Onu, C.E.; Nwabanne, J.T.; Ohale, P.E.; Asadu, C.O. Comparative analysis of RSM, ANN and ANFIS and the mechanistic modeling in eriochrome black-T dye adsorption using modified clay. *S. Afr. J. Chem. Eng.* **2021**, *36*, 24–42.
38. Deshwal, S.; Kumar, A.; Chhabra, D. Exercising hybrid statistical tools GA-RSM, GA-ANN and GA-ANFIS to optimize FDM process parameters for tensile strength improvement. *CIRP J. Manuf. Sci. Technol.* **2020**, *5*, 11.